Collapse of higher-order solute concentration moments in groundwater transport

Veljko Srzic,[1,2] Roko Andricevic,[2] Hrvoje Gotovac,[2] and Vladimir Cvetkovic[1]

Received 16 December 2012; revised 9 May 2013; accepted 18 June 2013; published 5 August 2013.

[1] In this paper, we use numerical simulations based on a Lagrangian framework to study contaminant transport through highly heterogeneous porous media due to advection and local diffusion (under local diffusion, we assume coupled effect of mechanical dispersion and molecular diffusion). The analysis of the concentration field is done for the case of a two-dimensional hydraulic conductivity domain representing the aquifer, with three log-conductivity structures that differ in spatial correlation. In addition to different conductivity structures, we focus our investigation on mild and highly heterogeneous porous media characterized by the values of hydraulic log-conductivity variance $\left(\sigma_Y^2\right)$ being equal to 1 and 8. In the concentration moment analysis, we show that a linear relationship exists between higher-order to second-order normalized concentration moments on a log-log scale up to the fourth-order moment. This leads to the important finding that moments of a higher than the second order can be derived based on information about the first two concentration moments only. Such a property has been observed previously for boundary-layer water channels, wind tunnels, and turbulent diffusion in open terrain and laboratory experiments. Normalized moments are shown to collapse for different types of hydraulic conductivity structures, Peclet (Pe) numbers and σ_Y^2 values. In the case of local diffusion absence, a linear log-log relationship is derived analytically and is set as a lower limit. The deviation from the lower limit is explained to be predominantly caused by the local diffusion, which needs time to evolve. In the case of local diffusion presence, we define the moment deriving function (MDF) to describe the linear log-log relationship between higher-order concentration moments to the second-order normalized one. Finally, the comparison between numerical results and those obtained from the Columbus Air Force Base Macrodispersion Experiment (MADE 1) is used to demonstrate the robustness of the moment collapse.

Citation: Srzic, V., R. Andricevic, H. Gotovac, and V. Cvetkovic (2013), Collapse of higher-order solute concentration moments in groundwater transport, *Water Resour. Res.*, *49*, 4751–4764, doi:10.1002/wrcr.20371.

1. Introduction

[2] In the turbulent diffusion field of research, many investigators were focused on analyzing the concentration probability density function (pdf) and its related moments. Those findings range from the exponential [*Lewis and Chatwin*, 1996; *Yee and Chan*, 1997b] distribution to the Clipped-Normal [*Yee and Chan*, 1997a, 1997b], generalized Pareto [*Lewis and Chatwin*, 1996; *Schopflocher and Sullivan*, 2002], Gamma [*Lewis and Chatwin*, 1996; *Klein and Young*; 2011], Clipped-Gamma [*Klein and Young*, 2011; *Yee and Chan*, 1997a; *Yee*, 2008], and α-β [*Mole*, 1995; *Yee and Chan*, 1997b] distribution. It is important to realize that investigators of the atmospheric turbulent diffusion problems had not only numerical tools at their disposal but also extensive data sets obtained through detailed concentration fluctuation experiments in open terrain [*Lewis and Chatwin*, 1996; *Klein and Young*, 2011; *Yee and Chan*, 1997a], wind tunnels [*Schopflocher and Sullivan*, 2005; *Yee et al*., 2006], and water channels [*Yee and Wilson*, 2000; *Yee et al*., 2006; *Yee*, 2008, 2009]. One of the general findings in these studies is the fact that higher-order concentration moments do provide valuable additional information for the shape of the concentration pdf.

[3] Furthermore, the studies conducted by *Yee* [2008, 2009] and *Yee and Chan* [1997a, 1997b], using a data set of large concentration fluctuations collected under different conditions, showed a remarkable collapse of data on a single curve when comparing various higher-order normalized concentration moments $\langle (c/C)^n \rangle$ ($n = 3$, 4, 5, 6, 7, and 8) versus the second-order normalized concentration moment $\langle (c/\langle C \rangle)^2 \rangle$. With c we denote the concentration variable while C presents the concentration ensemble mean.

[1]Department of Land and Water Resources, KTH-Royal Institute of Technology, Stockholm, Sweden.
[2]Department of Water Resources, Faculty of Civil Engineering, Architecture and Geodesy, University of Split, Split, Croatia.

Corresponding author: V. Srzic, Department of Land and Water Resources, KTH-Royal Institute of Technology, Stockholm, Sweden. (veljko.srzic@gradst.hr)

©2013. American Geophysical Union. All Rights Reserved.
0043-1397/13/10.1002/wrcr.20371

[4] Concentration moments of solute released through aquifers, atmosphere, and water channels have been of great interest in the last few decades. The analyses of concentration moments in heterogeneous aquifers have been considered in a few studies [*Andricevic*, 1998; *Bellin et al*., 1994; *Caroni and Fiorotto*, 2005; *Dagan and Fiori*, 1997; *Fiori and Dagan*, 2000; *Fiori*, 2003; *Fiorotto and Caroni*, 2002; *Kapoor and Kitanidis*, 1998]. In an early attempt to characterize groundwater contaminant transport, *Dagan* [1982] showed that in the absence of local diffusion and for point sampling, the concentration pdf is a two-state process of initial concentration, C_0, or zero. The same feature is valid even in the atmosphere and water channel flow. *Bellin et al*. [1994] analyzed the cumulative distribution function (cdf) and the first two concentration moments as a function of sampling size. In later works, local diffusion is considered and its influence is analyzed through the first two moments, concentration mean and variance [*Andricevic*, 1998; *Caroni and Fiorotto*, 2005; *Dagan and Fiori*, 1997; *Fiori and Dagan*, 1999, 2000; *Fiori*, 2003; *Fiorotto and Caroni*, 2002; *Tonina and Bellin*, 2008], in both Eulerian and Lagrangian frameworks. The calculation of concentration moments of an order higher than two is commonly constrained by a number of physical (number of measurements and its scale) and numerical reasons (number of realizations, extensive computational resources, and numerical accuracy). In order to avoid some of the above-mentioned facts, one needs to increase the number of realizations. This procedure is time consuming and reveals the necessity for finding effective tools that can determine higher-order moment values based on information about lower order ones.

[5] Knowledge of the statistical properties of concentration fluctuations in a moving plume is important in assessing the risk from adverse effects of certain highly toxic chemicals, ranging from industrial chemicals to even certain chemical warfare agents. Risk assessment studies require the knowledge of concentration fluctuations [*Andricevic et al*., 2012; *Tartakovsky*, 2007], which are described by one-point concentration pdf. At any point in space and time, the concentration pdf contains all the information about concentration fluctuations and embodies all the higher-order concentration moments.

[6] Following the first suggestion of a Beta distribution for the subsurface concentration made by *Fiori* [2001], *Caroni and Fiorotto* [2005] showed the applicability of Beta distribution and a good fit for Monte Carlo (MC) results conducted in 2-D heterogeneous aquifer. *Bellin and Tonina* [2007] confirmed results by *Caroni and Fiorotto* [2005] showing Ito Stochastic Differential Equation leads to Beta pdf. Also, in comparison with Gaussian and Lognormal distribution, Beta showed better features in order to capture the ensemble fluctuations. *Schwede et al*. [2008] reached very good agreement with Beta by semianalytical method even in 3-D, but for unity σ_Y^2 and multi-Gaussian (MG) field. Joint velocity-concentration pdf method has been developed by *Meyer et al*. [2010] and compared with results by *Caroni and Fiorotto* [2005] up to $\sigma_Y^2 = 2$. The accuracy of this method is shown to decrease for $Pe \leq 100$ when compared with standard MC. All the above-mentioned results indicate the asymmetric shape of the concentration pdf [*Cirpka et al*., 2011b], for a wide range of parameters. Although the Beta distribution has shown relatively good features in capturing concentration fluctuations phenomena, some limitations have been noted [*Bellin and Tonina*, 2007; *Caroni and Fiorotto*, 2005]. For the sometimes complex structure of the concentration field, the mean and variance may not be sufficient and higher-order statistical moments are required to accurately define the concentration pdf shape. Furthermore, most of the concentration findings in groundwater transport research to date have been focused on a lower range of aquifer heterogeneity $\left(\sigma_Y^2 < 2\right)$ and a common MG log-conductivity field.

[7] The objective of this paper is to investigate the features of the statistical properties of a plume spreading in a heterogeneous aquifer as manifested through the higher-order concentration moments (third and fourth), and their relationship to second-order normalized ones. In view of this, the question we pose is as follows: Does the concentration in a groundwater plume transported through aquifers of high heterogeneity, different *Pe* values and different log-conductivity fields exhibit a collapse of the higher-order concentration moments on the second-order concentration moment? If so, we can use this collapse feature to obtain moments of a higher order than the second one, solely from information about the first two moments.

[8] To address above questions, we will employ the two-dimensional Monte Carlo numerical experiments. Using our recently presented simulation methodology, Adaptive Fup Monte Carlo Method (AFMCM) [*Gotovac et al*., 2007, 2009a]; this methodology supports the Eulerian-Lagrangian formulation and separates the flow from the transport problem. A heterogeneous aquifer is modeled with a log-conductivity variance ranging from 1 to 8 (e.g., describing highly heterogeneous cases), including three fundamentally different log-conductivity fields [*Zinn and Harvey*, 2003], and *Pe* value ranging from 100 to 10,000.

2. Statement of the Problem and Methodology

[9] Consider incompressible and steady groundwater flow taking place through a heterogeneous aquifer, resulting in divergence free flow $\nabla \cdot \mathbf{v}(\mathbf{x}) = 0$. A velocity vector is defined on the finite volume, surrounding position vector $\mathbf{x}$, which corresponds to Darcy scale at any time t. In general, we fully follow the numerical procedure explained in detail in *Srzic et al*. [2013] and briefly summarized below for completeness.

[10] If a finite volume of a conservative tracer with corresponding mass is introduced into an aquifer, we rely on the mass conservation law in the form

$$\frac{\partial c(\mathbf{x},t)}{\partial t} = -\nabla \cdot [\mathbf{v}(\mathbf{x})c(\mathbf{x},t)] + \nabla \cdot [\mathbf{D}(\mathbf{x})\nabla c(\mathbf{x},t)] \qquad (1)$$

[11] The concentration scalar field is denoted by $c(\mathbf{x}, t)$ and defined as the contaminant mass per aquifer volume surrounding $\mathbf{x}$ at time t. $\mathbf{D}(\mathbf{x})$ is dispersion tensor, representing coupled effect of mechanical dispersion and molecular diffusion.

[12] For the solution of equation (1), the Random Walk Particle Tracking (RWPT) method is used to simulate contaminant transport of a conservative tracer in the form

$$\mathbf{X}_P(t+\Delta t) - \mathbf{X}_P(t) = [\mathbf{v}(\mathbf{X}_P;t) + \nabla \cdot \mathbf{D}(\mathbf{X}_P;t)] \cdot \Delta t + \mathbf{B}(\mathbf{X}_P;t) \cdot \xi(t)\sqrt{\Delta t} \tag{2}$$

where the first term on the right-hand side is the drift vector while the displacement matrix $\mathbf{B}(X_P;t)$ defines the strength of local diffusion, $\xi(t)$ presents a vector of independent, normally distributed random variables with zero mean and unit variance. Equation (2) presents the solution of the advection-dispersion equation presented in equation (1) as the number of particles tends to infinity [*Gardiner*, 1990].

[13] In the form of the backward random walk particle tracking (BRWPT) scheme, equation (2) can be used for calculating particle displacement except the starting position of each particle, which is located inside the sampling volume [*Caroni and Fiorotto*, 2005; *Fiorotto and Caroni*, 2002]. The number of particles N_P is distributed normally or uniformly inside a sampling volume, surrounding location x, and tracked back toward the source volume using equation (2). If n of total number of particles N_P released from sampling volume, in any time step Δt is found inside the source volume, the resident concentration [*Parker and van Genuchten*, 1984] can be evaluated as

$$c(\mathbf{x},t) = C_0 \frac{n}{N_P} \tag{3}$$

where C_0 presents the initial concentration and refers to a situation in which all released particles are found inside the source volume.

[14] The numerical procedure used here for the calculation of concentration values consists of four steps:

[15] 1. generating random hydraulic conductivity field with defined statistical properties using [*Bellin and Rubin*, 1996]

[16] 2. evaluation of Eulerian velocity and head field using AFMCM [*Gotovac et al*., 2007, 2009a] for numerical domain with defined boundary conditions solving flux balance equation

[17] 3. evaluating particles displacements in any time step using equation (2)

[18] 4. resident concentration evaluation using equation (3).

[19] The numerical method AFMCM [*Gotovac et al*., 2007, 2009a] used in this paper for the flow and transport problem solution is based on Fup basis functions with compact support (related to the other localized basis functions such as splines or wavelets) and the Fup collocation transform (FCT), which is closely related to the discrete Fourier transform needed for the multiresolution representation of all flow and transport variables. Fup basis functions and the FCT are presented in *Gotovac et al*. [2007]. Other improved Monte Carlo (MC) methodology steps were also utilized: (i) the Fup regularized transform (FRT) for data or function (e.g., log conductivity) approximations in the same multiresolution fashion as FCT, but computationally more efficient, (ii) the adaptive Fup collocation method (AFCM) for approximation of the flow differential equation, (iii) the backward random walk particle tracking algorithm based on the Runge-Kutta-Verner explicit time integration scheme and FRT, and (iv) MC statistics represented by Fup basis functions.

[20] In this paper, we use the numerical setup shown in Figure 1 for simulation of contaminant transport in order to analyze the influence of log-conductivity variance, *Pe* number, and different conductivity structure types on concentration moments. To minimize the impact of boundary conditions, transport is simulated inside an inner domain, $8I_Y$ from upper and lower no-flux boundaries, and $12I_Y$ away from left-side and right-side constant head boundaries. For the same numerical setup in the study conducted by *Gotovac et al*. [2009b], by inspection of velocity variance in both longitudinal and transversal directions, it is confirmed that the boundary effects are avoided even for highest $\sigma_Y^2 = 8$. In comparison, *Salandin and Fiorotto* [1998] used $4I_Y$ to minimize the boundary effects. Based on ensemble convergence study presented in detail in Appendix A, 2500 $\left(\sigma_Y^2 = 8\right)$ and 500 $\left(\sigma_Y^2 = 1\right)$ statistically independent contaminant transport realizations are generated by releasing 400 particles, uniformly distributed inside each of the 43 sampling volumes. The spatial discretization used in our model corresponds to $I_Y/4$ [*Gotovac et al*., 2009a; *Salandin and Fiorotto*, 1998], while the sampling volume is also set to be $I_Y/4$, except for the purpose of checking moment collapse convergence (Figures 4a and 4b). Heterogeneity grid is selected based on the study

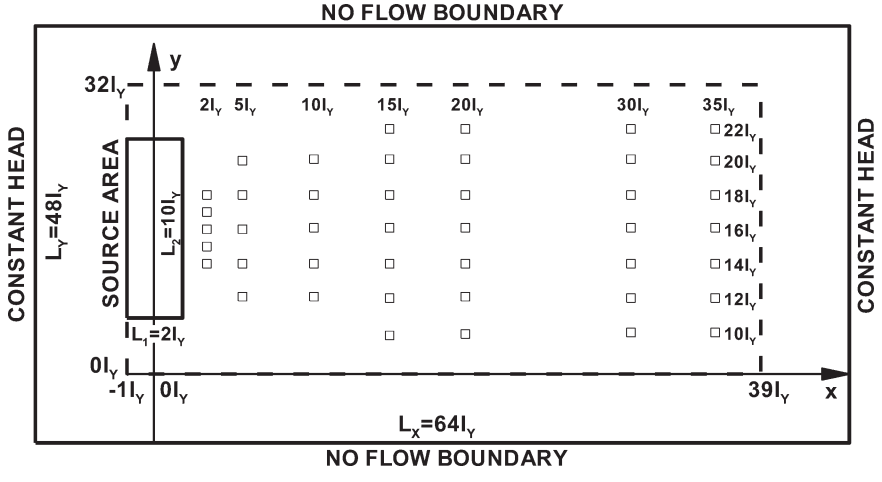

Figure 1. Numerical setup.

conducted in our previous paper [*Srzic et al*., 2013], where we demonstrated the sensitivity of the concentration moments to the grid scale in case of $\sigma_Y^2 = 8$. Our results rely on Figure 12 by *Gotovac et al*. [2009a], where they demonstrated that both Eulerian velocity component variances differ less than 4.5% when the number of cells per integral length is changed from 4 to 8 for $\sigma_Y^2 = 8$. Moreover, *Gotovac et al*. [2009a] in Figure 16 showed that the transversal displacement and the travel time pdf are almost identical for both discretization levels, $n = 4$ and 8. Our results correspond to σ_Y^2 being either 1 or 8 for three types of conductivity structures [*Zinn and Harvey*, 2003] with an isotropic Gaussian variogram. The log-conductivity structures we use here are generic and do not strictly provide information about any real case. The effects of local diffusion are analyzed for *Pe* 100 and 10,000. The latter value can be considered to describe advection-dominated transport. For purpose of numerical simulations dispersion tensor from equation (1) is assumed as isotropic one with constant value calculated by $D = UI_Y/Pe$. U denotes mean velocity. Regarding the backward random-walk particle-tracking scheme, the source dimension is set to be significantly larger than the sampling volume. Its dimension in the longitudinal direction is $L_1 = 2I_Y$, while in the transversal direction it is set equal to $L_2 = 10I_Y$. For the initial condition, the concentration inside the source area is uniformly distributed taking C_0 value, while outside the source area it is set to be equal to zero.

[21] All three hydraulic conductivity structures considered here have identical lognormal univariate conductivity distributions, as well as isotropic spatial covariance functions. The connectivity of the same log-conductivity patterns is interpreted as a possible consequence of the geological processes that generated the aquifer itself. The three structures differ in the pattern by which high-conductivity or low-conductivity regions are connected:

[22] 1. ConNected—CN field with well-connected high-conductivity channels, but poorly connected low and mean conductivity zones. This type of structure is characterized by an effective conductivity greater than the geometric mean and large variations in fluid velocity.

[23] 2. DisconNected—DN field with well-connected low conductivity zones such that mass transfer occurs through low value conductivity fields. This type of structure is characterized by an effective conductivity less than the geometric mean and smaller velocity variations.

[24] 3. Multi-Gaussian—MG field, where extreme conductivity values are poorly connected, while mean conductivity zones are well connected. This structure is (for the 2-D flow case) consistent with first-order theory.

3. Concentration Moment Collapse

3.1. Zero Local Diffusion Case

[25] In the case of advection only (local diffusion absence), the point concentration of a conservative tracer released from a source with uniformly distributed concentration C_0 is either equal to initial concentration C_0 or zero, depending on whether the sampler is located inside or outside of the solute body. Therefore, the concentration field must be characterized as a two-state process, taking values equal to zero or C_0. Without loss of generality, we here normalize the concentration by C_0, so that the concentration takes values equal to 0 or 1. Then, the concentration pdf possesses a bimodal feature and takes the following mathematical form

$$p(c;\mathbf{x},t) = \gamma_0(\mathbf{x},t)\delta(c(\mathbf{x},t)-1) + (1-\gamma_0(\mathbf{x},t))\delta(c(\mathbf{x},t)) \quad (4)$$

[26] The first term on the right-hand side (RHS) presents the probability of concentration to be equal to the concentration value inside a plume, while the second one presents the probability that the concentration value is zero, i.e., the sampling location is outside of the plume. Moreover, $\gamma_0(\mathbf{x},t)$ is a so-called intermittency factor, defined as a probability of concentration to be greater than zero, representing the situation in which the sampling point is within the plume [*Chatwin and Sullivan*, 1989]. The absolute moments of concentration pdf presented in equation (4) are expressed as

$$m_n(\mathbf{x},t) = \int_0^1 c(\mathbf{x},t)^n p(c;\mathbf{x},t)dc = \gamma_0(\mathbf{x},t); n \geq 1 \quad (5)$$

[27] In the case of zero local diffusion and point sampling, intermittency is equal to the concentration mean like all other higher moments. This can occur because there is no mechanism that causes concentration reduction.

[28] Let us examine the possible relationship, already observed in turbulent diffusion in open terrain and laboratory experiments, water channel, and wind tunnel experiments [*Lewis and Chatwin*, 1996; *Klein and Young*; 2011, *Yee and Chan*, 1997a; *Schopflocher and Sullivan*, 2005; *Yee and Wilson*, 2000, *Yee et al.*; 2006, *Yee*, 2008, 2009], of higher-order normalized concentration moments to the second-normalized moment:

$$\frac{m_n(\mathbf{x},t)}{(m_1(\mathbf{x},t))^n} = \left(\frac{m_2(\mathbf{x},t)}{(m_1(\mathbf{x},t))^2}\right)^{n-1}; n > 2 \quad (6)$$

[29] After introducing moment values from equation (5) in both sides of equation (6), we can confirm the above equality, which will serve as the lower limit relationship for the case where local diffusion effects are present. Equation (6) states that all higher-order moments are directly related to the first two concentration moments. Taking the logarithm of equation (6), all higher moments are linearly (with the slope factor equal to $n-1$) related to the ratio of the second to the first concentration moment.

3.2. Nonzero Local Diffusion Case

[30] Consider now the case with a finite *Pe* number indicating nonzero local diffusion as a mechanism that reduces concentration values inside a plume; thus, at any sampling location one can observe that concentration values are between 0 and 1 (again utilizing normalization by C_0). If sampling is located inside the plume boundaries, the observed value is greater than zero $(c(\mathbf{x},t) \in \langle 0,1])$, while otherwise the observed concentration value outside the plume is equal to 0. Because equation (4) is limited to account for binary concentration values only, we wish to modify it such that all concentration values inside a plume boundary can be captured. To this end, we propose

introducing a new function $g(c;\mathbf{x},t)$ that generalizes equation (4) in the following form:

$$p(c;\mathbf{x},t) = \gamma(\mathbf{x},t)g(c;\mathbf{x},t) + (1-\gamma(\mathbf{x},t))\delta(c(\mathbf{x},t)) \quad (7)$$

where the intermittency factor is now denoted by $\gamma(\mathbf{x},t)$ to present the probability of concentration to be greater than zero (as in the advection-only case), but now accounting for local diffusion; in this case, equation (5) is not applicable. The function $g(c;\mathbf{x},t)$ possesses a pdf property (finite integral over the range bounded by 0 and 1, equal to 1—easily proved by integrating equation (7)) and presents the probability of concentration values greater than zero to occur, or in other words, the function $g(c;\mathbf{x},t)$ presents a pdf of nonzero concentration values. Although $g(c;\mathbf{x},t)$ possesses a pdf property, $p(c;\mathbf{x},t)$and $g(c;\mathbf{x},t)$ are not the same because of different values of samples taken into account. The number of samples for $g(c;\mathbf{x},t)$ is equal to the total number of nonzero $c(\mathbf{x},t)$ values, while in the case of $p(c;\mathbf{x},t)$, sampling over all concentration values (zero and nonzero) is made. After scaling $g(c;\mathbf{x},t)$ by $\gamma(\mathbf{x},t)$ and by adding zero values probability (second part of the right-hand side in equation (7)), equation (7) is satisfied. Therefore, we use the same concept in equation (7) as in equation (4), separating the meandering effect from the concentration values inside the plume, caused by advection and local diffusion.

[31] In the case of nonzero local diffusion, we modify equation (6) by using equation (7) and obtain a new relationship between the higher concentration moments to the second normalized concentration moment as

$$\frac{m_n(\mathbf{x},t)}{\left(m_1(\mathbf{x},t)\right)^n} = \beta_n(\mathbf{x},t)\left(\frac{m_2(\mathbf{x},t)}{\left(m_1(\mathbf{x},t)\right)^2}\right)^{n-1} \quad ; \quad n>2 \quad (8)$$

where a function $\beta_n(\mathbf{x},t)$ is introduced to account for the influence of local diffusion. $\beta_n(\mathbf{x},t)$ is referred to as the moment deriving function (MDF), and its value will be examined using numerical simulations. Equation (8) implies that higher normalized concentration moments are still related to the second concentration moment but are now scaled with the function $\beta_n(\mathbf{x},t)$, depending on the heterogeneity structure, σ_Y^2, and local diffusion. The following section will analyze how $\beta_n(\mathbf{x},t)$ behaves under different conditions.

[32] From the application viewpoint, under the real aquifer conditions we can measure only the function $g(c;\mathbf{x},t)$ and its moments in a single realization (e.g., MADE [*Zheng et al*., 2010]). Therefore, it is important to verify equation (8) even in such cases. We start from the absolute moments of $p(c;\mathbf{x},t)$

$$m_n^p(\mathbf{x},t) = \gamma(\mathbf{x},t)\int_0^1 c(\mathbf{x},t)^n g(c;\mathbf{x},t)\mathrm{d}c + (1-\gamma(\mathbf{x},t))\int_0^1 c(\mathbf{x},t)^n\delta(c(\mathbf{x},t))\mathrm{d}c \quad (9)$$

[33] Due to the properties of integrating Dirac's delta function, second part on the RHS vanishes and we get

$$m_n^p(\mathbf{x},t) = \gamma(\mathbf{x},t)m_n^g(\mathbf{x},t) \quad (10)$$

[34] After introducing equation (10) into equation (8), it is obvious that independent of concentration moments used $m_n^p(\mathbf{x},t)$ or $m_n^g(\mathbf{x},t)$, equality presented by equation (8) is satisfied while at the same time $\beta_n(\mathbf{x},t)$ is unaffected regardless of the moments used ($m_n^p(\mathbf{x},t)$ or $m_n^g(\mathbf{x},t)$). This indicates that the moment collapse feature, equation (8) should be applicable even in field experiments, a point that will be investigated in section 4.2.

4. Results

4.1. Concentration Moments Collapse

[35] The numerical procedure presented in section 2 was used to produce concentration values resulting from the advection-dispersion processes. For all 43 sampling locations presented in Figure 1 and a dimensionless time domain ranging between 0 and 100, normalized concentration values are evaluated. To prove the linear log-log relationship defined by equation (8) between higher-order and second-order normalized concentration moments derived in the previous section, a few selected results are presented in Figures 2a–2c (third-normalized versus second-normalized moments) and Figures 3a–3c (fourth-normalized versus second-normalized moments). Each scattergram consists of 172,000 normalized concentration values. It can be seen that the lower limit considered in the case of zero local diffusion has never been failed and all numerical values are positioned above this lower limit. Some differences between different hydraulic conductivity structure types (MG, CN, and DN), *Pe* values, and log-conductivity variances are presented in the scattergrams. To capture the properties of each scattergram, we use a linear regression model to calculate correlation coefficient ρ_n and MDF (β_n) values for all considered cases up to the sixth moment order in Tables 1 and 2. Note that we use here MDF without spatial and temporal notation, because it presents the collapse for all dimensionless snapshots and sampling locations at once. Subscript *n* denotes the order of higher concentration moments in a linear relationship with a second-order normalized one. Linear regression analysis is performed with a slope equal to the lower limit case, while the only difference appears in the ordinate value (representing β_n).

[36] σ_Y^2 is shown to be dominant in influencing ρ_n and β_n values. Higher σ_Y^2 causes increased Lagrangian integral scale as shown by several studies [*Gotovac et al*., 2009b, Figure 8a; *Meyer and Tchelepi*, 2010, Figures 8a and 8b; *Salandin and Fiorotto* 1998, Figures 5a and 5b]. In combination with slow advection as a consequence of portion of mass being stacked in low-velocity areas, the plume spreading is enhanced. This is more obvious in the case of CN field compared with MG and especially DN structure. The CN structure is characterized by significant correlation values of extremely high velocities characterizing connected high log-conductivity channels, but also with very large surfaces of isolated low log-conductivity zones that enhance retention. This makes the plume more dispersed over a larger aquifer area and results with larger surface area available for contaminant transfer to the zones outside the plume boundaries, reducing concentration values. In addition, Figures 4a and 4b couples the effect of sampling

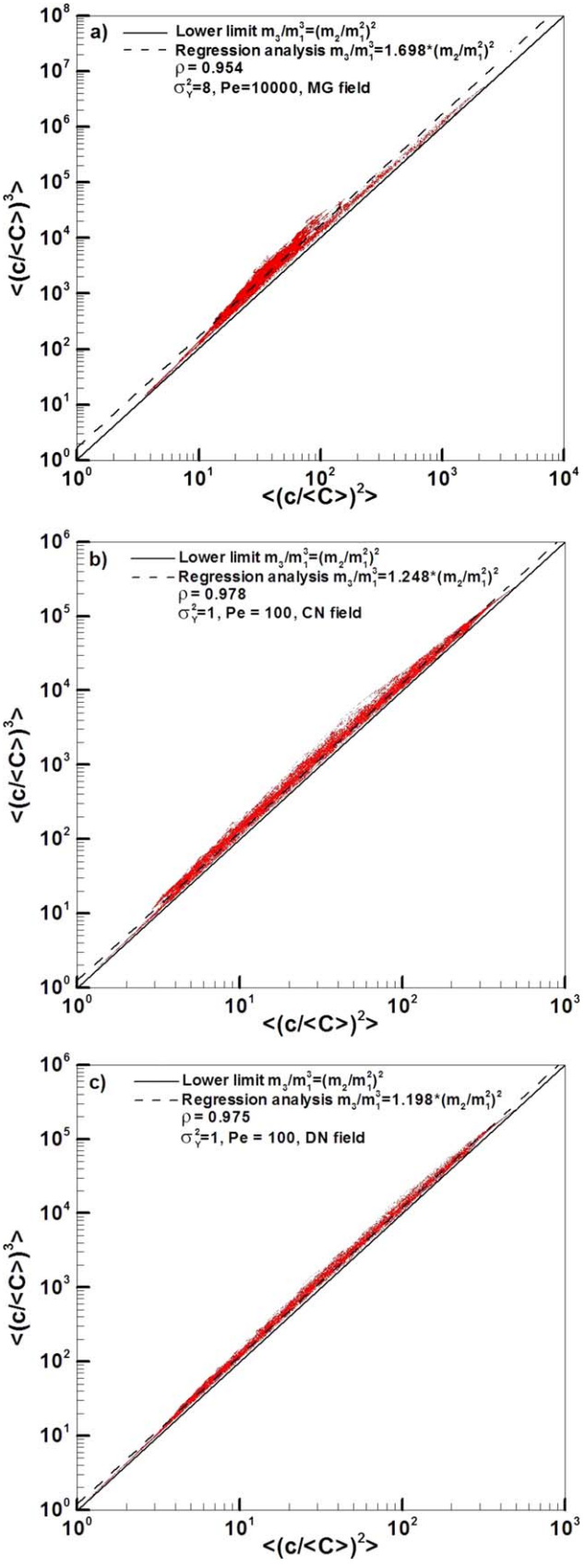

Figure 2. Normalized concentration third versus second moment (a) ln K variance = 8, Pe = 10,000, MG field, (b) ln K variance = 1, Pe = 100, CN field, and (c) ln K variance = 1, Pe = 100, DN field.

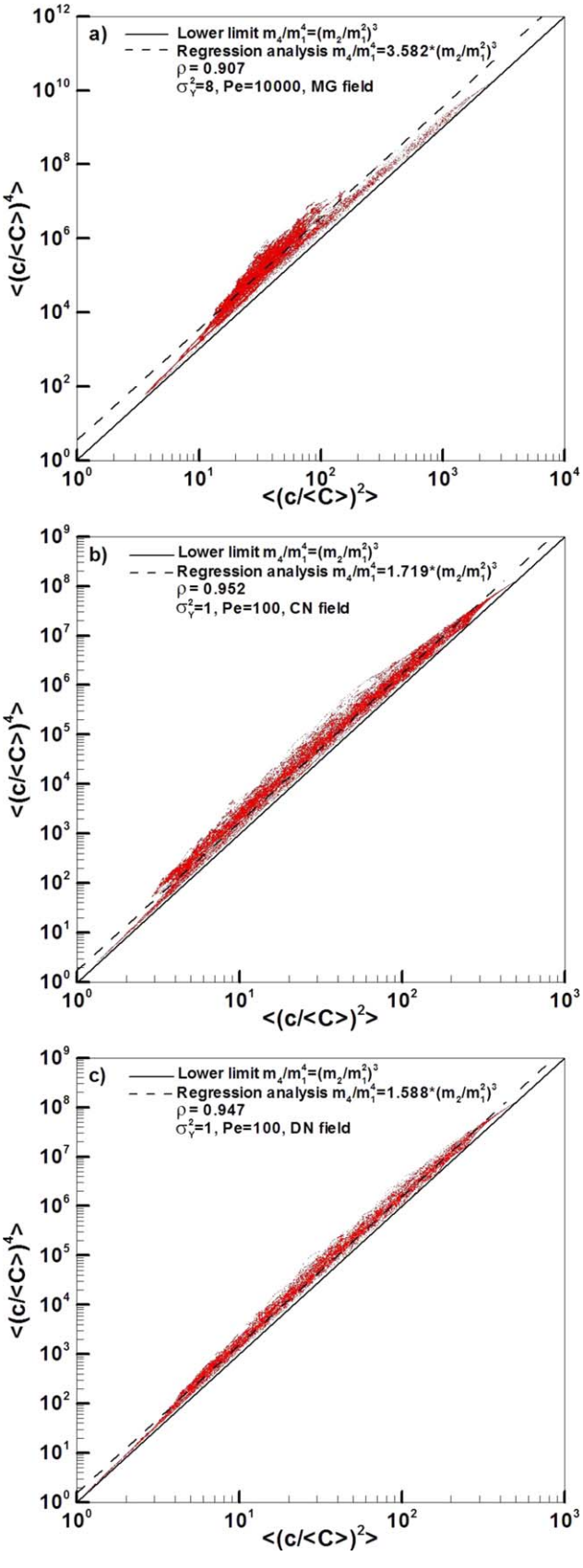

Figure 3. Normalized concentration fourth versus second moment: (a) ln K variance = 8, Pe = 10,000, MG field, (b) ln K variance = 1, Pe = 100, CN field, and (c) ln K variance = 1, Pe = 100, DN field.

Table 1. Moment Deriving Function (MDF) and Correlation Coefficient Values Numerical Results in Case of Third, Fourth, Fifth and Sixth Order for ln K Variance = 1

Field	CN		MG		DN	
Peclet Number	100	10,000	100	10,000	100	10,000
ρ_3	0.978	0.977	0.973	0.977	0.975	0.976
β_3	1.248	1.177	1.241	1.191	1.198	1.180
ρ_4	0.952	0.951	0.941	0.950	0.947	0.948
β_4	1.719	1.485	1.693	1.534	1.588	1.499
ρ_5	0.933	0.932	0.916	0.931	0.926	0.927
β_5	2.496	1.939	2.427	2.054	2.112	1.983
ρ_6	0.918	0.917	0.897	0.916	0.912	0.911
β_6	3.736	2.584	3.584	2.814	2.950	2.684

volume with local diffusion, particularly for the MG field. In the case of pure advection and point sampling (lower limit), $\beta_n = 1$ for all n as explained in the previous section. A relatively small sampling volume ($I_Y/64$) for the advection-only case confirms that numerical and statistical errors in our computational methodology are fairly small, even for a high heterogeneity case. To achieve a lower limit for MDF in case of pure advection, the sampling size must be very small (less than $I_Y/64$). This is particularly true for high heterogeneity cases and higher-order concentration moments. Therefore, the sampling volume cannot be ignored under certain transport conditions, due to the introduction of additional mixing [*Andricevic*, 1998; *Bellin et al*., 1994; *Tonina and Bellin*, 2008].

[37] The *Pe* number as a measure of local diffusion presence has a key influence in defining β_n values. Higher *Pe* values cause the scattergram to be closer to the lower limit, and thereby β_n closer to one. For smaller *Pe* values, local diffusion starts to dominate, and the deviation from the lower limit case is more pronounced. These features are presented in Figures 2a–2c, 3a–3c, 4a, and 4b. In the case of higher-order normalized moments, the deviation from $\beta_n = 1$ is much more pronounced, which is in agreement with *Srzic et al*. [2013]. The high correlation coefficients ρ_n show that the moment collapse property of each scattergram is present, regardless of different *Pe* number, σ_Y^2 value, and hydraulic conductivity structures.

[38] To further explain the properties of scattergrams, it is necessary to closely examine the scatter structure. The $\beta_n(x,t)$ is generally characterized by spatial and temporal dependencies in the same way as the moment values

Table 2. Moment Deriving Function (MDF) and Correlation Coefficient Values Numerical Results in Case of Third, Fourth, Fifth and Sixth Order for ln K Variance = 8

Field	CN		MG		DN	
Peclet Number	100	10,000	100	10,000	100	10,000
ρ_3	0.938	0.950	0.972	0.954	0.947	0.954
β_3	1.808	1.788	1.701	1.698	1.589	1.537
ρ_4	0.877	0.905	0.947	0.907	0.904	0.918
β_4	4.521	4.073	3.675	3.582	3.152	2.768
ρ_5	0.838	0.875	0.931	0.873	0.880	0.896
β_5	13.381	10.390	9.277	8.361	7.013	5.368
ρ_6	0.812	0.853	0.919	0.848	0.864	0.881
β_6	43.386	28.108	25.325	20.599	16.620	10.839

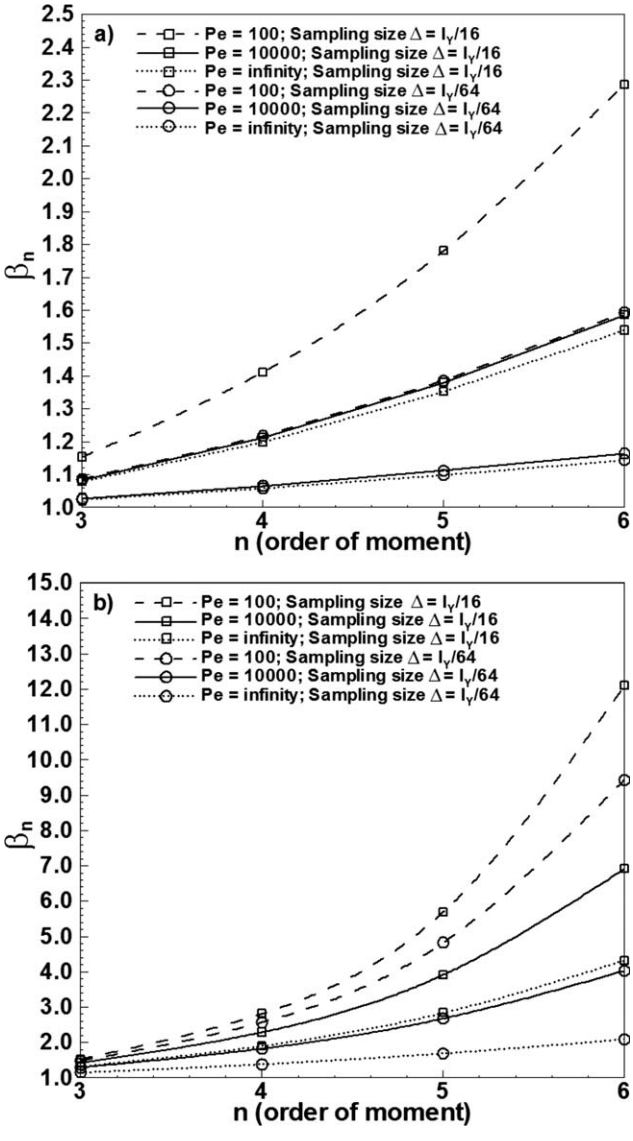

Figure 4. MDF value versus order of moment related with second-order normalized moment depending on sampling volume: (a) unit log-conductivity variance, MG field and (b) log-conductivity variance equal to 8, MG field.

$m_n(x,t)$, while the local diffusion process is time dependent, evolving with time increases. Since $\beta_n(x,t)$ is predominantly dependent on the *Pe* number (local diffusion), in Figures 5a and 5b, we present the relationship between higher-order (third and fourth order) normalized moments and the second-order moment normalized for three randomly selected snapshots (at $tU/I_Y = 5$, 20, and 50, where the mean velocity is denoted by U) in the case of a CN field, $\sigma_Y^2 = 8$ and $Pe = 10{,}000$. For each snapshot, we calculate $\beta_n(t)$ with linear regression and evaluate the correlation coefficient ρ_n. Figures 5a and 5b show two very important findings:

[39] 1. Regardless of how many sampling locations the plume covers, the $\beta_n(\mathbf{x},t)$ values show very weak spatial dependence due to the significant correlation, i.e. $\beta_n(\mathbf{x},t) \rightarrow \beta_n(t)$.

[40] 2. The $\beta_n(t)$ values increase with the plume travel time and converge approximately to a constant value at

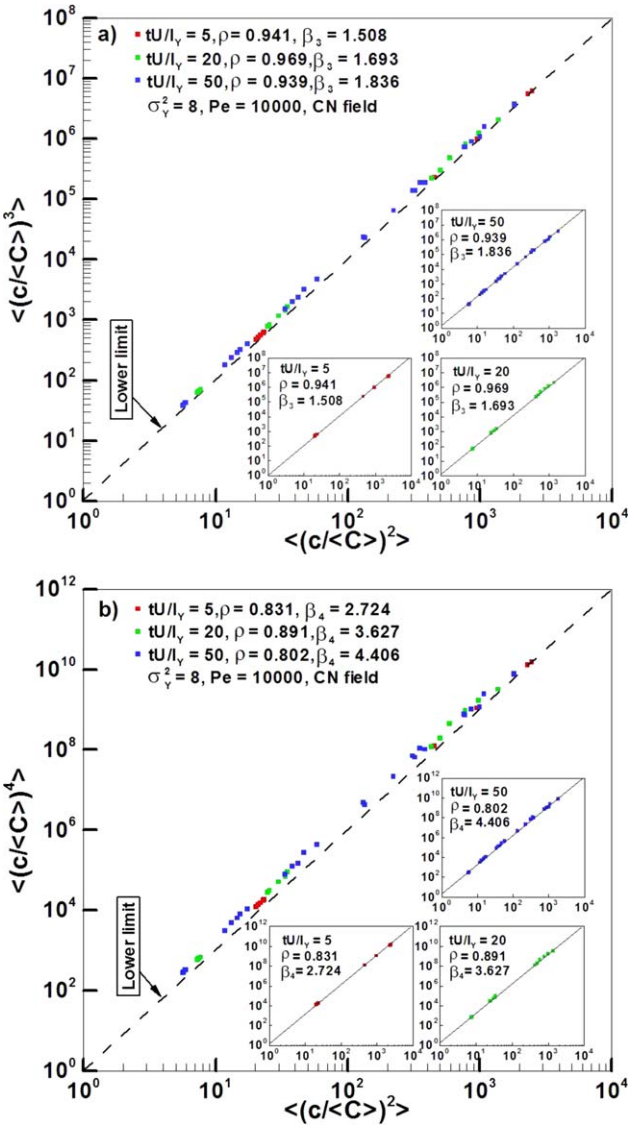

Figure 5. (a) Selected snapshots ($tU/I_Y = 5$, 20, and 50) normalized concentration third-order versus second-order moment, ln K variance = 8, $Pe = 10{,}000$, CN field and (b) selected snapshots ($tU/I_Y = 5$, 20 and 50) normalized concentration fourth-order versus second-order moment, ln K variance = 8, $Pe = 10{,}000$, CN field.

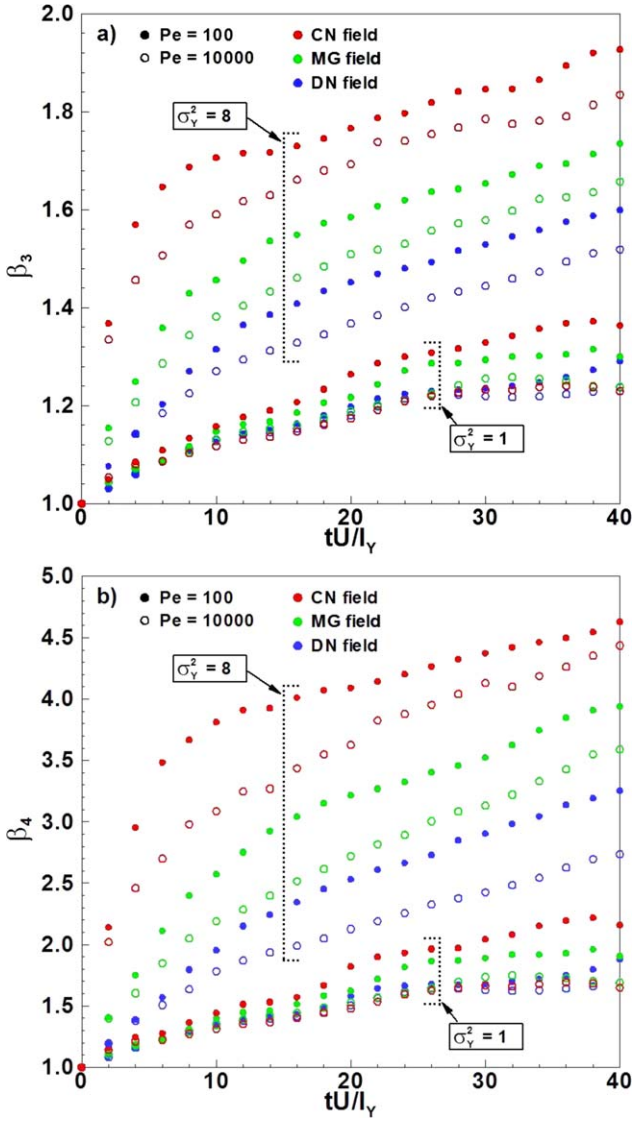

Figure 6. MDF values as a function of dimensionless time: (a) second versus third normalized moment and (b) second versus fourth normalized moment.

large time. This temporal dependence coincides with the local diffusion evolution in time.

[41] Thus, we can consider MDF from now on only time dependent ($\beta_n(t)$) with a significant correlation coefficient indicating the remarkable moment collapse property.

[42] Figures 6a and 6b presents the development of $\beta_n(t)$ for the relationship of third- and fourth-normalized concentration moments to the second-normalized concentration moment. It is evident that for high σ_Y^2, $\beta_n(t)$ increases due to the increase in concentration fluctuations resulting in larger surface area of the plume with stronger concentration gradients, which in turn enhance the local diffusion effect. Increasing $\beta_n(t)$ results in a shift of moment collapse away from the lower pure advection minimum as seen in Figures 5a and 5b. After some time of plume development (e.g., after $tU/I_Y = 40$), it can be seen that the $\beta_n(t)$ asymptotically converges to its stable value ($\beta_3(t) = 1.25$ and $\beta_4(t) = 1.6$ for $\sigma_Y^2 = 1$, while $\beta_3(t) = 1.65$ and $\beta_4(t) = 3.5$ for $\sigma_Y^2 = 8$). After $tU/I_Y = 40$, the plume starts to exceed the domain resulting in fewer sampling locations in our simulations, which in turn reduces the MDF. The conductivity structure types do not significantly affect MDF values, even for higher-order moments (we checked up to sixth order but the results are not shown). Generally, the highest MDF values are characterized in the case of the CN field. Transport in the case of a CN field occurs through both highly connected zones (preferential channels) [*Boggs et al.*, 1992; *Rehfeldt et al.*, 1992; *Wen and Gomez-Hernandez*, 1998; *Zheng et al.*, 2010; *Zinn and Harvey*, 2003] where the concentration field is characterized by sharp gradients, as well as through the low permeable zones where the mass amount is stacked. As we noted previously, the consequence is enhanced plume spreading with increased plume surface

available for mass transfer to the neighboring zones primarily by transverse local diffusion [*Cirpka and Kitanidis*, 2000; *Cirpka et al*., 2011a]. On the other hand, as expected, the plume characterizing DN field has a more compact form compared with CN and MG structures and exhibits the lowest MDF values.

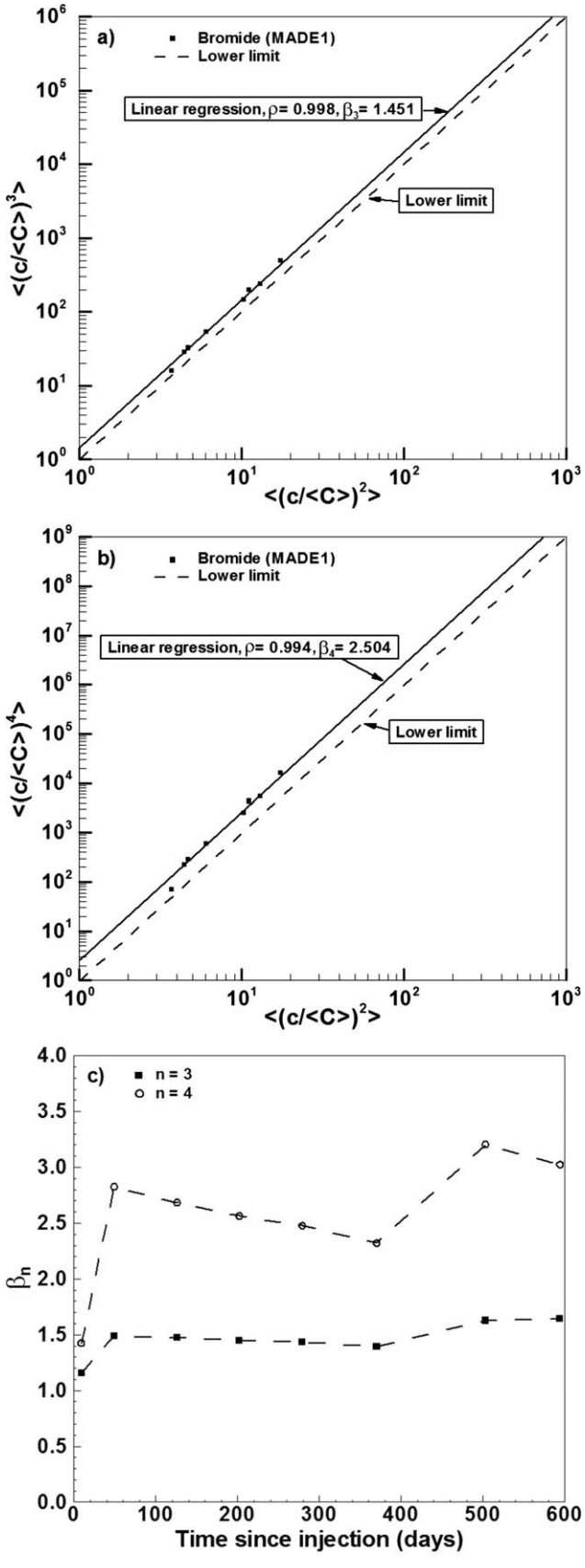

Figure 7. MADE—MDF values derived from Conservative Bromide tracer normalized spatially integrated moments for eight different snapshots taken 9, 49, 126,202, 279, 370, 503, and 594 days since injection: (a) second versus third normalized moment, (b)second versus fourth normalized moment, and (c) third-order and fourth-order MDF values plot versus real time.

4.2. Field Experiment and Moment Collapse Feature

[43] In subsurface flow and transport studies, it is very rare to find concentration statistics based on field measurements. This is especially true for the higher concentration moments, which provide information about the concentration fluctuations and the shape of the plume. In this section, the presented feature of normalized higher concentration-moment collapse will be examined using concentration data from the conservative Bromide tracer test obtained from the macrodispersion experiment (MADE 1) at Columbus Air Force Base in Mississippi [*Boggs et al*., 1992; *Rehfeldt et al*., 1992]. The natural gradient experiment was performed in a shallow alluvial aquifer consisting of heterogeneous, lenticular deposits of sand and gravel. The experiment was initiated with the injection of 10.07 m^3 of groundwater containing bromide with an initial concentration set to 2500 mg/L [*Boggs et al*., 1992]. Eight snapshots were conducted over a period of approximately 20 months. The time interval between plume samplings ranges from 5 to 19 weeks. A network of 258 sampling wells, each with up to 30 sampling points in the vertical direction, was used to monitor the tracer plumes in three dimensions.

[44] The absolute moment values of $g(c;\mathbf{x},t)$ and $p(c;\mathbf{x},t)$ differ by an intermittency factor, and log-log moment collapse as defined by equation (8) is valid for both pdfs $g(c;\mathbf{x},t)$ and $p(c;\mathbf{x},t)$. We consider under real aquifer conditions only concentration values greater than zero (or more precisely above detected threshold) inside the plume and evaluate the pdf $g(c;\mathbf{x},t)$. Adopting the assumption that the plume in each of the eight snapshots fulfills the ergodic conditions (through the time plume covers from two (first snapshot) to more than 20 (eighth snapshot) correlation lengths in longitudinal direction [*Adams and Gelhar*, 1992]), spatially integrated normalized concentration moments [*Andricevic*, 1998] are calculated for each snapshot excluding concentration values below the threshold limit equal to 0.1 mg/L for snapshots 1–4 and 0.01 mg/L for snapshots 5–8 [*Boggs et al*., 1992] (due to the different measurement technique used). Evaluated moments are normalized, and the ratio between higher-order (third and fourth) and second-order normalized moment is displayed in Figures 7a and 7b. Bromide data analysis shows that $\beta_3(t)$ is stabilizing at 1.451, while $\beta_4(t)$ reaches 2.504 with correlation coefficients 0.998 and 0.994. The field data examination shows a striking agreement with the numerical simulations when compared with Figures 6a and 6b. The log-conductivity variance characterizing the Columbus site varies depending on the conductivity scale; *Rehfeldt et al*. [1992] reported an

overall variance of the horizontal log-conductivity equal to 4.5 with correlation length 12.8 m in longitudinal and 1.6 m in transversal direction, the study conducted by *Harvey and Gorelick* [2000] at the submeter scale raises up the value to 20 for the single location (borehole), while results made by *Bohling et al*. [2012] based on direct-push techniques at the centimeter scale indicate log-conductivity variance close to 7. The sampling volume, used in the MADE site, is much smaller than correlation length [*Boggs et al*., 1992], so the assumption of point sampling is valid. Including the fact that the *Pe* value in field experiments varies in the range of 10^2-10^3 [*Fiori and Dagan*, 1999], qualitatively good agreement in β_n values has been achieved.

[45] It is also interesting to analyze the first data point from bromide concentration in Figure 7c. Namely, this point corresponds to only 9 days since injection began and the plume has not been developed yet; consequently, the effect from local diffusion is comparatively small. All other data points reflect a well-developed plume and some form of equilibrium between advection in stretching the plume and local diffusion as a smoothing mechanism. This balance between advection and local diffusion has been previously observed [*Andricevic*, 1998] and seems to be closely related to the MDF in reaching the constant value.

[46] In Figure 7c, we reinforce our discussion above, showing how quickly the field data present the stabilization of MDF. This is particularly true for $\beta_3(t)$ while for the fourth moment some increased fluctuations are noticed for snapshots, but still, global stabilization and increased form are observable.

[47] The fact that MDF values in the limit $t \rightarrow 0$ approach unity clearly indicates that the early transport time is advection dominated and MDF is close to 1 for all moments. Only when the plume starts to stretch out, providing local diffusion with more surface area to become an important process, the MDF values start to increase. The flattening out at some later time is connected with a balancing between the advection strength (function of σ_Y^2) and local diffusion.

5. Discussion

[48] In this study, we determine the linear log-log relationship between the higher-order (third and fourth) normalized concentration moments to the second-order normalized concentration moment for subsurface transport (Figures 2 and 3) independent of sampling location and time since injection. This moment collapse feature was already observed in the atmospheric turbulent diffusion problems [*Yee and Chan*, 1997a, 1997b; *Yee*, 2008, 2009], but its behavior and peculiarities for the groundwater problems and comparison with some field data [*Boggs et al*., 1992; *Zheng et al*., 2010] are provided in this study. The fact that there exists such a higher moment collapse relative to the second order one is of great importance for further studies focusing on concentration pdf and consequently the probabilistic risk assessment [*Andricevic et al*., 2012; *Tartakovsky*, 2007].

[49] To reach the functional relationship between higher normalized concentration moments to the second order one, we start with the concentration pdf presented with two terms in equation (7). The first one corresponds to the non-zero concentration found within the plume, and the second one presents the probability of zero concentration to occur. In the case of zero local diffusion, the moment collapse feature follows exactly equation (6) having a linear coefficient equal to $n-1$ on the log-log scale.

[50] The case of pure advection and the point sampling with uniform initial concentration we use as the base case, as well as the proof of moment collapses robustness, since the exact relationship equation (6), with β_n equal to unity, which is identical to the correlation coefficient. In this case, we conclude that the moment collapse (or the scaling feature of the normalized concentration moments) exists independent of the flow field or structure. Furthermore, the no-diffusion case implies that the moment collapse cannot be constrained by the physical problem dimensionality. Although our study has been conducted in 2-D, the concentration pdf equation (4) in the case of local diffusion absence and the point sampling still captures all possible concentration values (zero or C_0) regardless of problem dimensionality. In other words, the moment collapse presented by equation (6) holds even in 3-D. The higher-order concentration moment collapse occurs independent of the media in which pure advective transport takes place. In fact, a number of published works deal with concentration moment collapse in the atmosphere, open terrain and laboratory measurements, water channels, and wind tunnels. Finally, we note that the injection mode does not affect equation (6), as it affects for instance the travel time and/or breakthrough curves [*Demmy et al*., 1999; *Gotovac et al*., 2010; *Jankovic and Fiori*, 2010], in the case of pure advection, point sampling, and uniform initial concentration; this is because all concentration moments are equal to intermittency $\gamma_0(\mathbf{x},t)$. Although in case of in flux injection mode, the initial mass is distributed proportionally to the velocity field along the source line, according to the definition of the flux-averaged concentration [*Demmy et al*., 1999; *Parker and van Genuchten*, 1984], the initial condition is interpreted as a constant C_0 since the ratio between the mass flux and water flux is constant.

[51] When local diffusion acts together with advection (as in natural subsurface transport), we introduce the new function called Moment Deriving Function (β_n) to describe the influence of local diffusion. The relationship in equation (8) is examined numerically for finite *Pe* values and evaluated using field data from the MADE site. Our results suggest that the new function $\beta_n(t)$ is a function of time; in the limit $t \rightarrow 0$, it is equal to 1 (advection only) and starts to increase due to the combined effect of advection and local diffusion. Even when analyzed with a different *Pe*, different log-conductivity variances and three different log-conductivity structures, $\beta_n(t)$ behaves in a consistent manner, showing robustness when evaluated as a function of transport time. Both σ_Y^2 and the log-conductivity structure affect MDF through the local diffusion. Although $\beta_n(t)$ is computed by linear regression model (with the assumption that the slope is equal to 1 in the zero local diffusion case) significant correlation is observed for each snapshot. The correlation coefficients obtained for each snapshot in Figures 5a and 5b reflect the MDF's dependence primary on time with significant correlation coefficient values that decrease as the order of normalized moment increases. The decreased correlation is to be expected since the

fluctuations of the moments increase with increasing order. The variability of the correlation coefficients for each snapshot and higher-order moment needs to be investigated additionally in order to determine the moment collapse accuracy and eventual cause of deviations from the unity correlation coefficient, accounting for different possible sources of error (numerical, statistical).

[52] To demonstrate the influence of such errors and accuracy of the numerical procedure used, we presented results in Figures 4a and 4b, where we clearly show the convergence of the MDF toward unity as the *Pe* is increased and the sampling volume decreased; in other words, the convergence of the MDF toward the advection and point sampling case is demonstrated. However, it is important to note that even for the smallest sampling used, some concentration reduction is present due to the finite sampling size.

[53] The potential relevance of the moment collapse is its uniqueness, since we showed that it can be applied to whole concentration data sets including zero values as well when applied to just nonzero values that are the only ones measured in reality: independent of the data set used, MDF maintains the same value. This was confirmed by introducing equation (10) into equation (8). We also examined the behavior of $\beta_n(t)$ by evaluating concentration data obtained from the MADE site (first experiment), exposing the striking feature of moment collapse. The interesting finding is that the $\beta_n(t)$ behaves in the same way as found in the numerical simulations. Assuming ergodicity was necessary to compare spatially integrated moment values with ensemble ones obtained from numerical simulations. Although the longitudinal plume dimension ranges between 2 and more than 20 correlation lengths, the MDF calculated from MADE data sets is shown to have the characteristic qualitative features as those obtained by numerical simulations. Additionally, observed concentration at MADE is flux averaged [*Boggs et al*., 1992] with the continuous uniform pulse injection (48.5 h), with a minimal disturbance to the natural flow field (corresponds to in flux injection mode). These facts reinforce the robustness of the MDF for different conditions and dimensionality even with transient head boundary conditions.

[54] The suggested concentration pdf models used in previous investigations [*Bellin et al*., 1994; *Bellin and Tonina*, 2007; *Caroni and Fiorotto*, 2005; *Fiorotto and Caroni*, 2002; *Klein and Young*; 2011; *Lewis and Chatwin*, 1996; *Schopflocher and Sullivan*, 2002; *Yee and Chan*, 1997a, 1997b] are a priori defined analytically. These analyses have been made by fitting field results, laboratory measurements, or numerically generated concentration values to the above analytical pdf models that are regularly defined by the first two concentration moments at least. The examination of conditions under which the pdf is adequate to characterize the concentration fluctuations was commonly constrained by log-conductivity variance up to 2 and the MG fields in the subsurface [*Bellin et al*., 1994; *Bellin and Tonina*, 2007; *Caroni and Fiorotto*, 2005; *Fiorotto and Caroni*, 2002]. The concept of MDF presented in this paper enables one to use information about the first two concentration moments (based on collected or measured data) to produce higher-order moments that are necessary to capture the non-Gaussian pdf shape [*Bellin and Tonina*, 2007; *Caroni and Fiorotto*, 2005; *Cirpka et al*., 2011b; *Dentz and Tartakovsky*, 2010; *Meyer et al*., 2010; *Schwede et al*., 2008].

[55] For higher-order concentration moments calculated by the moment collapse, the moment inversion technique enables evaluation of the concentration pdf for a variety of heterogeneity structures and variably *Pe* values. The accuracy of the higher-order concentration moments calculated from the moment collapse approximation and their separate contribution to the concentration pdf is a part of our ongoing research. The preliminary results indicate the decreased contribution of the concentration moment to the pdf, as the moment order increases. Also, the results suggest increased number of moments in case of a poorly mixed plume, usually in the near zone. For a well-mixed plume, it appears that just three moments are sufficient under specific conditions for relatively accurate estimates of the pdf.

[56] The possible improvements and further studies for finite *Pe*, we see in increased number of samplings in order to better capture the moment fluctuations for the MDF calculation. Although we showed the validity and the robustness of the moment collapse for a wide range of conditions, the MDF calculation is affected by the setup parameters, like source size, sampling volume, log-conductivity variance and structure, injection mode, and dimensionality; so all the combinations require separate determination of MDF through time in order to apply the moment collapse for the higher-order moments calculation for finite *Pe*. Although we believe that the combination of advection heterogeneity and the local diffusion leads to the scaling of the concentration moments, the possible influence of other mechanisms relevant in the subsurface, such as retention and/or decay, needs to be further investigated.

6. Conclusions

[57] Although the moment collapse has been demonstrated previously in the turbulent diffusion field, to the best of our knowledge, this paper is the first one dealing with its properties and peculiarities in groundwater transport. We base our study on a combination of analytical and numerical results for pure advection and advection combined by local diffusion, respectively. Throughout the manuscript, we offer a large set of results that support our findings and explain the phenomenon referred to as moment collapse when applied to groundwater contaminant transport. Also, we establish a relation of the moment collapse with the physical mechanisms acting on the concentration field. Below, we summarize the highlights arising from this study:

[58] 1. When advection is the only present mechanism and the sampling is a point with uniform initial concentration, the higher-order concentration moments collapse was shown to be exact and robust for a wide range of setup parameters with the constant MDF value equal to unity. This holds for all moments up to order of n.

[59] 2. If local diffusion is present as an additional mechanism to advection, the MDF is primarily a temporal function, increasing from one following the local diffusion evolution.

[60] 3. Both the log-conductivity variance and structure affect the MDF through the local diffusion causing a concentration reduction due to different plume features that are controlled by heterogeneity and the spatial correlation of the log-conductivity patterns.

[61] 4. The sampling volume involves artificial concentration reduction (smoothing) due to spatial averaging. This causes additional deflection of the MDF from the lower limit (i.e., the advection case) even for small sampling size.

[62] 5. MADE data confirmed the robustness and the validity of the moment collapse under conditions that strictly differ from those of our numerical simulations. This reinforces the main merit of the moment collapse; its existence and applicability in real cases that arise from the insensitivity to the moments used (m_n^p or m_n^g) and prevailing boundary conditions.

Appendix A: Monte Carlo Convergence

[63] For investigation of higher-order normalized concentration moments convergence, we use numerical setup presented in Figure 1. The number of flow and transport realizations (N_R) is increased, starting from 10, until convergence in third-order and fourth-order normalized moment is reached. As CN conductivity field is characterized by highest spatial variability in velocity field [*Zinn and Harvey*, 2003], we select it as representative. Convergence tests are done for both $\sigma_Y^2 = 1$ and 8, and Pe values equal to 100 and 10,000. In Figures A1a and A1b, we show the results for $\sigma_Y^2 = 8$ and $Pe = 100$. Figure A1a presents relatively rapid convergence of third-order normalized moment, independent of the distance from the source and position inside the plume boundaries (plume core or plume fringes). After $N_R = 1500$, the third moment shows very low sensitivity, changes in moment values are less than 6%. Finally, the difference between moment values for $N_R = 2400$ and 2500 is less than 1%. Similar behaviour is observed even for fourth-order normalized moment values in Figure A1b. For $N_R = 1500$, the difference is less than 10% reducing to 2.5%. To summarize, convergence test of third-order and fourth-order normalized moments showed that 2500 Monte Carlo realizations are sufficient to achieve stable moment values for $\sigma_Y^2 = 8$. In the case of lower heterogeneity level $(\sigma_Y^2 = 1)$, this number is 500.

[64] In order to reach stability of $\beta_n(t)$ values, we use the number of Monte Carlo (N_R) realizations defined in previous convergence analysis of higher-order moments and check for $\beta_3(t)$ and $\beta_4(t)$ values. Three different dimensionless snapshots ($tU/I_Y = 2$, 20, and 50) are selected that show convergence of MDF for CN and DN fields and $\sigma_Y^2 = 8$. In Figures A2a and A2b, it is shown that convergence for both $\beta_3(t)$ and $\beta_4(t)$ is first observed for the earliest snapshot independent of the heterogeneity structure due to the increased plume meandering effect as the time evolves. In the case of $\sigma_Y^2 = 1$, MDF up to fourth order is shown to be stable for 500 Monte Carlo realizations (Figure A2c).

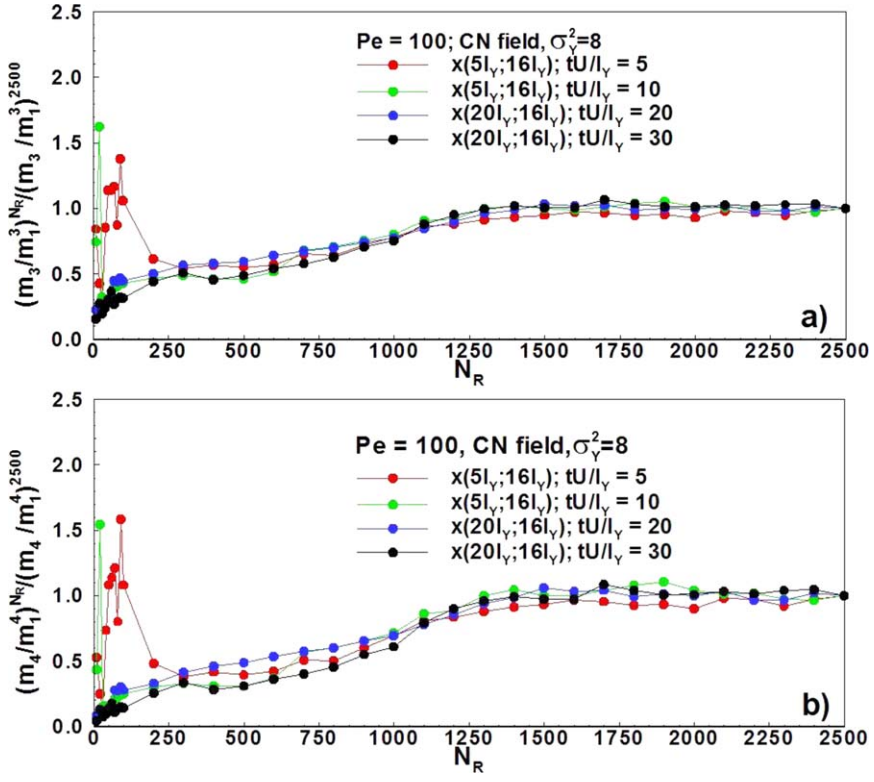

Figure A1. $Pe = 100$, ln K variance $= 8$, CN field: (a) convergence of third-order normalized concentration moment and (b) convergence of fourth-order normalized concentration moment.

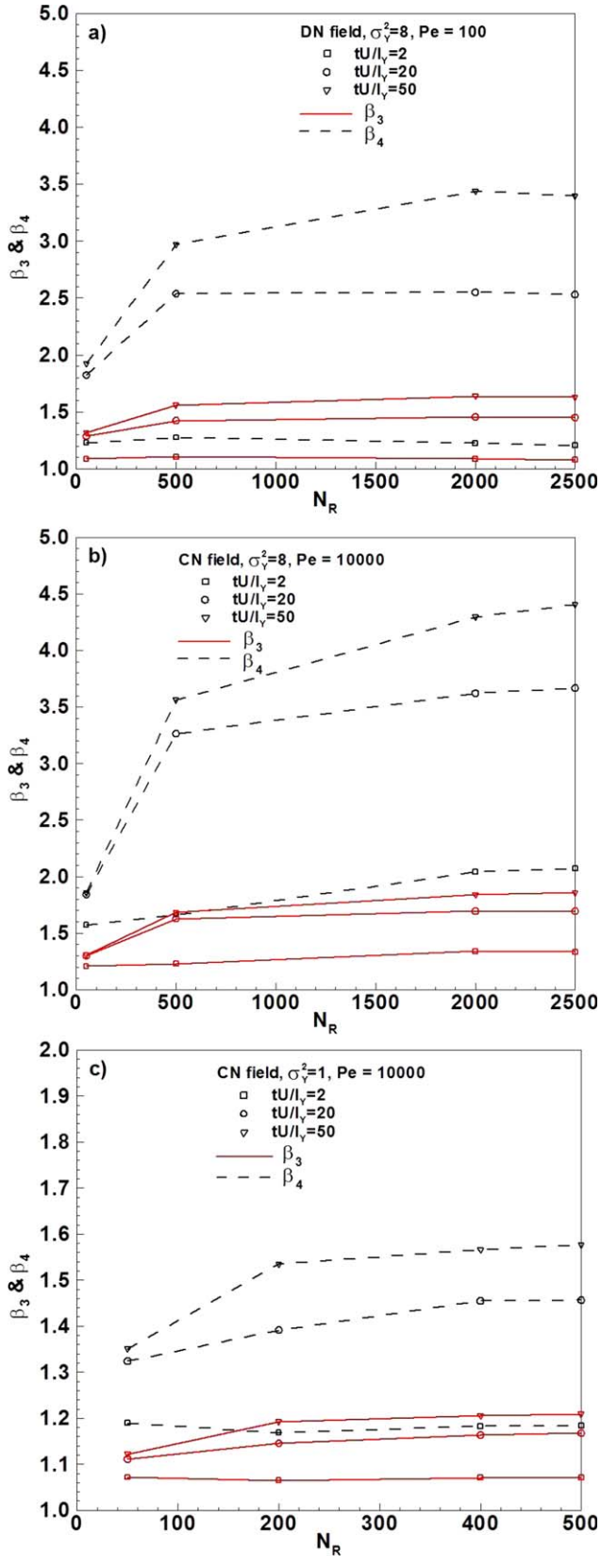

Figure A2. Convergence of MDF value: (a) $Pe = 100$, ln K variance = 8, DN field, (b) $Pe = 10{,}000$, ln K variance = 8, CN field, and (c) $Pe = 10{,}000$, ln K variance= 1, CN field.

References

Adams, C. W., and L. W. Gelhar (1992), Field study of dispersion in a heterogeneous aquifer: 2. Spatial moment analysis, *Water Resour. Res.*, *28*(12), 3293–3307.

Andricevic, R. (1998), Effects of local dispersion and sampling volume on the evolution of concentration fluctuations in aquifers, *Water Resour. Res.*, *34*(5), 1115–1129.

Andricevic, R., V. Srzic, and H. Gotovac (2012), Risk characterization for toxic chemicals transported in aquifers, *Adv. Water Res.*, *36*, 86–97, doi:10.1016/j.advwatres.2011.04.009.

Bellin, A., and Y. Rubin (1996), Hydrogen: A spatially distributed random field generator for correlated properties, *Stochastic Hydrol. Hydraul.*, *10*(4), 253–278.

Bellin, A., and D. Tonina (2007), Probability density function of non-reactive solute concentration in heterogeneous porous formations, *J. Contam. Hydrol.*, *91*,109–125.

Bellin, A., Y. Rubin, and A. Rinaldo (1994), Eulerian-Lagrangian approach for modeling of flow and transport in heterogeneous geological formations, *Water Resour. Res.*, *30*(11), 2913–2924.

Boggs, J. M., S. C. Young, and L. M. Beard (1992), Field study of dispersion in a heterogeneous aquifer: 1. Overview and site description, *Water Resour. Res.*, *28*(12), 3281–3291.

Bohling, G. C., G. Liu, S. J. Knobbe, E. C. Reboulet, D. W. Hyndman, P. Dietrich, and J. J. Butler Jr. (2012), Geostatistical analysis of the centimetre-scale hydraulic conductivity variations at the MADE site, *Water Resour. Res.*, *48*, W02525 doi:10.1029/2011WR10791.

Caroni, E., and V. Fiorotto (2005), Analysis of concentration as sampled in natural aquifers, *Transp. Porous Media*, *59*, 19–45.

Chatwin, P. C., and P. J. Sullivan (1989), The intermittency factor of scalars in turbulence, *Phys. Fluids*, *A1*(4), 761–763.

Cirpka, O. A., and P. Kitanidis (2000), Characterization of mixing and dilution in heterogeneous aquifers by means of local temporal moments, *Water Resour. Res.*, *36*(5), 1221–1236.

Cirpka, O. A., F. P. J. de Barros, G. Chiogna, M. Rolle, and W. Nowak (2011a), Stochastic flux-related analysis of transverse mixing in two dimensional heterogeneous porous media, *Water Resour. Res.*, *47*, W06515, doi:10.1029/2011WR010279.

Cirpka, O. A., F. P. J. de Barros, G. Chiogna, and W. Nowak (2011b), Probability density function of steady state concentration in two-dimensional heterogeneous porous media, *Water Resour. Res.*, *47*, W11523, doi:10.1029/2011WR010750.

Dagan, G. (1982), Stochastic modeling of groundwater flow by unconditional and conditional probabilities: 2. The solute transport, *Water Resour. Res.*, *18*(4), 835–848.

Dagan, G., and A. Fiori (1997), The influence of pore-scale dispersion on concentration statistical moments in transport through heterogeneous aquifers, *Water Resour. Res.*, *33*(7), 1595–1605.

Demmy, G., S. Berglund, and W. Graham (1999), Injection mode implications for solute transport in porous media: Analysis in a stochastic Lagrangian framework, *Water Resour. Res.*, *35*(7), 1965–1973.

Dentz, M., and D. M. Tartakovsky (2010), Probability density functions for passive scalars dispersed in random velocity fields, *Geophys. Res. Lett.*, *37*, L24406, doi:10.1029/2010GL045748.

Fiori, A. (2001), The Lagrangian concentration approach for determining dilution in aquifer transport: Theoretical analysis and comparison with field experiments, *Water Resour. Res.*, *37*(12), 3105–3114.

Fiori, A. (2003), An asymptotic analysis for determining concentration uncertainty in aquifer transport, *J. Hydrol.*, *284*, 1–12.

Fiori, A., and G. Dagan (1999), Concentration fluctuations in transport by groundwater: Comparison between theory and field experiment, *Water Resour. Res.*, *35*(1), 105–112.

Fiori, A., and G. Dagan (2000), Concentration fluctuations in aquifer transport: A rigorous first order solution and applications, *J. Contam. Hydrol.*, *45*, 139–163.

Fiorotto, V., and E. Caroni (2002), Solute concentration statistics in heterogeneous aquifers for finite Peclet numbers, *Transp. Porous Med.*, *48*, 331–351.

Gardiner, C. W. (1990), *Handbook of Stochastic Methods for Physics, Chemistry and The Natural Sciences*, Springer, New York.

Gotovac, H., R. Andricevic, and B. Gotovac (2007), Multi resolution adaptive modeling of groundwater flow and transport, *Adv. Water Res.*, *30*(5), 1105–1126.

Gotovac, H., V. Cvetkovic, and R. Andricevic (2009a), Adaptive Fup multi resolution approach to flow and advective transport in highly

heterogeneous porous media: Methodology, accuracy and convergence, *Adv. Water Res.*, *32*, 885–905.

Gotovac, H., V. Cvetkovic, and R. Andricevic (2009b), Flow and travel time statistics in highly heterogeneous porous media, *Water Resour. Res.*, *45*, W07402, doi:10.1029/2008WR007168.

Gotovac, H., V. Cvetkovic, and R. Andricevic (2010), Significance of higher moments for complete characterization of the travel time probability density function in heterogeneous porous media using the maximum entropy principle, *Water Resour. Res.*, *46*, W05502, doi:10.1029/2009WR008220.

Harvey, C., and S. M. Gorelick (2000), Rate-limited mass transfer or macrodispersion: Which dominates plume evolution at the Macrodispersion Experiment (MADE) site?, *Water Resour. Res.*, *36*(3), 637–650.

Jankovic, I., and A. Fiori (2010), Analysis of the impact of injection mode in transport through strongly heterogeneous aquifers, *Adv. Water Res.*, *33*, 1199–1205.

Kapoor, V., and P. K. Kitanidis (1998), Concentration fluctuations and dilution in aquifers, *Water Resour. Res.*, *34*(5), 1181–1193.

Klein, P. M., and D. T. Young (2011), Concentration fluctuations in an downtown urban area. Part I: Analysis of Joint Urban 2003 full-scale fast-response measurements, *Environ. Fluid Mech.*, *11*, 23–42.

Lewis, D. M., and P. C. Chatwin (1996), A three-parameter PDF for the concentration of an atmospheric pollutant, *J. Appl. Meteorol.*, *36*, 1064–1075.

Meyer, D. W., and H. A. Tchelepi (2010), Particle-based transport model with Markovian velocity processes for tracer dispersion in highly heterogeneous porous media, *Water Resour. Res.*, *46*, W11552, doi:10.1029/2009WR008925.

Meyer, D. W., P. Jenny, and H. A. Tchelepi (2010), A joint velocity-concentration PDF method for tracer flow in heterogeneous porous media, *Water Resour. Res.*, *46*, W12522, doi:10.1029/2010WR009450.

Mole, N. (1995), The $\alpha - \beta$ model for concentration models in turbulent flows. *Environmetrics*, *6*, 559–569.

Parker, J. C., and M. Th. van Genuchten (1984), Flux-averaged and volume-averaged concentrations in continuum approaches to solute transport, *Water Resour. Res.*, *20*(7), 866–872.

Rehfeldt, K. R., J. M. Boggs, and W. L. Gelhar (1992), Field study of dispersion in a heterogeneous aquifer: 3. Geostatistical analysis of hydraulic conductivity, *Water Resour. Res.*, *28*(12), 3309–3324.

Salandin, P., and V. Fiorotto (1998), Solute transport in highly heterogeneous aquifers, *Water Resour. Res.*, *34*(5), 949–961.

Schopflocher, T. P., and P. J. Sullivan (2002), A mixture model for the PDF of a diffusing scalar in a turbulent flow, *Atmos. Environ.*, *36*, 4405–4417.

Schopflocher, T. P., and P. J. Sullivan (2005), The relationship between skewness and kurtosis of a diffusing scalar, *Boundary Layer Meteorol.*, *115*, 341–358.

Schwede, R. L., O. A. Cirpka, W. Nowak, and I. Neuweiler (2008), Impact of sampling volume on the probability density function of steady state concentration, *Water Resour. Res.*, *44*, W12433, doi:10.1029/2077WR006668.

Srzic, V., V. Cvetkovic, R. Andricevic, and H. Gotovac (2013), Impact of aquifer heterogeneity structure and local diffusion on solute concentration uncertainty, *Water Resour. Res.*, *49*, doi:10.1002/wrcr.20314, in press.

Tartakovsky, D. M. (2007), Probabilistic risk analysis in subsurface hydrology, *Geophys. Res. Lett.*, *34*, L05404, doi:10.1029/2007GL029245.

Tonina, D., and A. Bellin (2008), Effects of pore scale dispersion, degree of heterogeneity, sampling size, and source volume on the concentration moments of conservative solutes in heterogeneous formations, *Adv. Water Resour.*, *31*, 339–354.

Wen, X. H., and J. J. Gomez-Hernandez (1998), Numerical modelling of macrodispersion in heterogeneous media: A comparison of multi-Gaussian and non multi-Gaussian models, *J. Contam. Hydrol.*, *30*, 129–156.

Yee, E. (2008), The concentration probability density function with implications for probabilistic modeling of chemical warfare agent detector responses for source reconstruction, Technical Report, Def. and Res. Dev., Canada.

Yee, E. (2009), Probability law of concentration in plumes dispersing in an urban area, *Environ. Fluid Mech.*, *9*, 389–407.

Yee, E., and R. Chan (1997a), A simple model for the probability density function of concentration fluctuations in atmospheric plumes, *Atmos. Environ.*, *31*(7), 991–1002.

Yee, E., and R. Chan (1997b), Comments on ''Relationship between higher moments of concentration and of dose in turbulent dispersion,'' *Boundary Layer Meteorol.*, *82*, 341–351.

Yee, E., and D. J. Wilson (2000), A comparison of the detailed structure in dispersing tracer plumes measured in grid-generated turbulence with a meandering plume model incorporating internal fluctuations, *Boundary Layer Meteorol.*, *94*, 253–296.

Yee, E., R. M. Gailis, A. Hill, T. Hildermann, and D. Kiel (2006), Comparison of wind-tunnel and water channel simulations of plume dispersion through a large array of obstacles with a scale field experiment, *Boundary Layer Meteorol.*, *121*, 389–432.

Zheng, C., M. Bianco, and S. M. Gorelick (2010), Lessons learned from 25 years of research at the MADE site, *Ground Water*, *49*, 649–662, doi:10.1111/j.1745.6584.2010.00753.

Zinn, B., and C. F. Harvey (2003), When good statistical models of aquifer heterogeneity go bad: A comparison of flow, dispersion, and mass transfer in connected and multivariate Gaussian hydraulic conductivity fields, *Water Resour. Res.*, *39*(3), 1051–1070, doi:10.1029/2001WR001146.